EUROPEAN
JOURNAL OF
MECHANICS
B/FLUIDS

Near-wall measurements of turbulence statistics in a fully developed channel flow with a novel laser Doppler velocity profile sensor

Katsuaki Shirai [*], Christian Bayer, Andreas Voigt, Thorsten Pfister, Lars Büttner, Jürgen Czarske

Chair of Measurement and Testing Techniques, Department of Electrical Engineering and Information Technology, Dresden University of Technology, Helmholtzstraße 18, 01069, Dresden, Germany

Abstract

This paper reports on the measurements of the near-wall turbulence statistics in a fully developed channel flow. The flow measurements were carried out with a novel laser Doppler velocity profile sensor with a high spatial resolution. The sensor provides both the information of velocity and position of individual tracer particles inside the measurement volume. Hence, it yields the velocity profile inside the measurement volume, in principle, without the sensor being mechanically traversed. Two sensor systems were realized with different techniques. Typically the sensor has a relative accuracy of velocity measurement of 10^{-3} and the spatial resolution of a few micrometers inside the measurement volume of about 500 µm long. The streamwise velocity was measured with two independent sensor systems at three different Reynolds number conditions. The resulting turbulence statistics show a good agreement with available data of direct numerical simulations up to fourth order moment. This demonstrates the velocity profile sensor to be one of the promising techniques for turbulent flow research with the advantage of a spatial resolution more than one magnitude higher than a conventional laser Doppler technique.
© 2007 Elsevier Masson SAS. All rights reserved.

Keywords: Turbulent flow; Channel flow; Velocity profile; Near wall; Turbulence statistics; Laser Doppler; Velocity profile sensor; Spatial resolution

1. Introduction

In the last decades a lot of efforts have been put in the investigation of the statistical behavior of turbulent boundary layers. The approaches have been both from experimental as well as numerical simulations and they provided precious information on the mechanisms and the structures of turbulence. However, there still remain open discussions toward filling the gap among theories, experimental and numerical simulations and real flows at high Reynolds number conditions. One of such is the existence of universality and scaling of turbulence statistics in a high Reynolds number flow. Proper scaling of mean velocity profile in a turbulent boundary layer has been still in discussion. The difficulty to investigate the topic remains mainly due to the lack of spatial resolution of both measurement techniques and nu-

merical simulations at high Reynolds number conditions. Continuous progress of computers and numerical simulation schemes would afford to simulate higher Reynolds number flows. On the other hand, experimental techniques have also been in progress particularly in optical techniques such as particle image velocimetry (PIV). Recently, PIV using a long-range microscope was applied to boundary layer with a spatial resolution of about 1 μm [1] and an extended technique of optical coherence tomography with a resolution better than 70 μm was proposed for velocity measurement in the vicinity of the wall [2]. However, existing experimental techniques are, in general, known to suffer from the spatial averaging effect when the scale of interest becomes relatively small compared to the sensing area of the sensor. Besides, the applicability of a technique based on analogy is questionable in a complex turbulent flow such as a boundary layer with adverse pressure gradient or/and strong three dimensionality.

Laser Doppler velocity profile sensor has been proposed by Czarske et al. [3,4] to overcome the spatial averaging effect of conventional laser Doppler anemometry (LDA). With the velocity profile sensor, a high spatial resolution down to sub-micrometers range has been reported by experimental as well as theoretical investigations. Since the sensor does not require any analogy to achieve the high spatial resolution, its applicability is not restricted to some specific types of flows. Recently, the real spatial resolution in a fluid flow of about 3.5 μm was demonstrated in a test measurement of a microchannel [5]. The feasibility of the sensor for the mean and rms (=root-mean square) velocities was reported on a turbulent channel flow [6], however, the results were highly contaminated by intense noise mainly caused by the instability of the laser source. The noise could not be excluded since it occurred in the same frequency range as the measurement of Doppler frequency took place. Spurious frequency caused by the laser noise was recorded as if it had been from real flow velocity. The results showed discernible deviation from the generally reported distribution even though the deviations were within the measurement uncertainties. There were also suspicious effects possibly caused by the insufficiently controlled boundary condition at the measurement location. The measurement was carried out at the channel exit which was directly opened to the laboratory atmosphere. Hence, there could be some effects caused by the sudden expansion of the flow.

In this paper we report on the recent measurement results of turbulence statistics with improved systems of the velocity profile sensor as well as a carefully prepared flow boundary conditions. Two independent sensor systems were built up with major improvements on optics and electronics for stable operation. The statistics are reported up to fourth order moment at three different Reynolds number conditions and compared with available direct numerical simulation (DNS) data.

2. Experimental apparatus and procedures

2.1. Channel flow

The flow to be measured was the turbulent boundary layer in a fully developed channel flow. The basic flow configuration was the same as reported in [6,7]. The wind tunnel was a blowing type and the working fluid was air at the laboratory temperature. The temperature was monitored and it was found that there was a drift of air temperature beyond certain rotational speed of the blower. In such a case, flow measurement was started after running the tunnel for a few hours. The air temperature change in the channel was $\pm 1\,^\circ$C at maximum during the measurements. For tracer particles, di-ethylhexyl sebacate (DEHS) was seeded from the upstream of the blower inlet using a commercial atomizer. The particle size was estimated from the technical data of the atomizer to be polydispersed around the mean particle diameter of 0.3 μm, which assures the tractability to the flow. The cross-sectional dimensions of the channel were 5×60 cm (aspect ratio of 1:12), which was sufficient to be considered as two-dimensional flow referring to [8]. The measurements were carried out at 6.2 m downstream from the channel inlet (corresponds to $248h$; $h = 2.5$ cm: channel half-width), where the flow was expected to be fully developed. Along the centerline of the channel, wall static pressure taps were equipped for monitoring the pressure gradient in the streamwise direction. The fully developed condition was confirmed concerning the static pressure from about 2.5 m ($= 100h$) downstream the inlet by the linear pressure gradient along the streamwise direction.

In the measurement section, a pair of glass plates was attached flush to both the top and the bottom walls of the channel to have an optical access and not to disturb the flow as shown in Fig. 1. The sensor was attached at the bottom side and the forward scattered signals were detected from the top side of the channel. Beam stops were used to block the direct beams from the sensor preventing the saturation of the photo-detectors. In former time, a single glass plate was attached to the end of the channel [6]. Measurements were carried out close to the channel exit assuming the
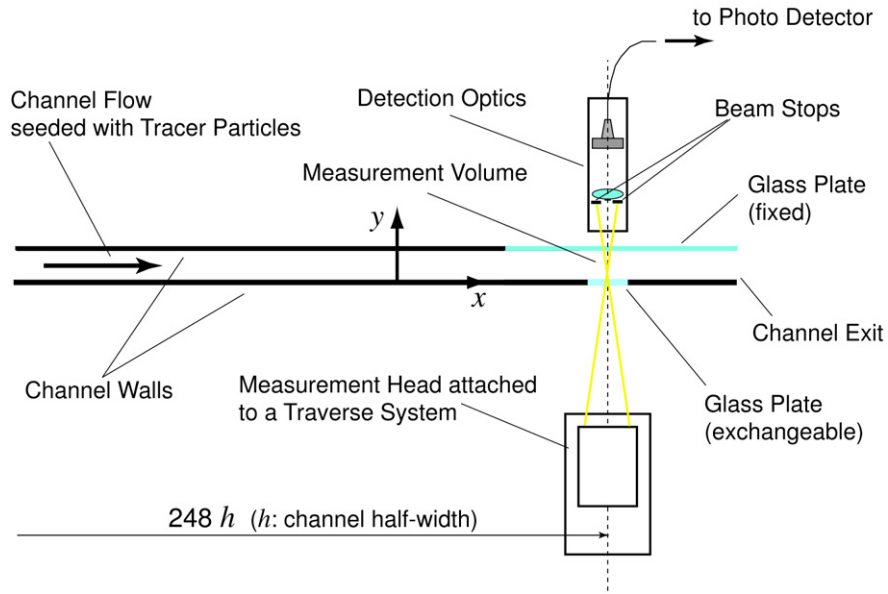
Fig. 1. Flow measurement configuration at the channel flow in a forward scatter regime ($Re_\tau = 420$). The velocity profile sensor was attached perpendicular to the wall with the advantage of a high spatial resolution in the direction of optical axis.

flow did not change from inside the channel. However, the flow faced a sudden change at the measurement location because it was opened directly to the ambient air at the channel exit. This was supposed to be the reason for the deviation of the velocity distribution compared to generally reported ones in the former measurement. Therefore, two sides of the channel walls at the channel exit were exchanged to a pair of glass plates for the present measurement. The measurement location was at the distance of about $12h$ upstream from the channel exit to avoid the effect of sudden expansion there. In the present flow measurement two different configurations of glass plates at the channel bottom wall were used for different flow conditions as described in detail in Section 2.4. One was to use a small glass window with good optical quality of $\lambda/4$ (λ: wavelength of incident light). The glass window was attached flush to the wall surface of the flow made of aluminum. The other was to use a large glass plate (fused silica) with ordinary quality covering the whole measurement section. The detection side (channel upper wall) was covered with a glass plate made of fused silica.

2.2. Velocity profile sensor

The flow measurements were carried out with a novel laser Doppler velocity profile sensor. The principle of the sensor is based on the use of two fringe systems in a single measurement volume. Since the details of the principle are described in the former papers [3,4], only the essence is described here. In contrast to a conventional laser Doppler technique, the profile sensor employs two pairs of beams with non-parallel fringe systems as shown in Fig. 2. The combination of diverging and converging fringe systems is suitable for maximizing the spatial resolution. The diverging and converging fringes are formed by shifting the position of the beam waists in forward and backward directions from the focal plane. The measured pair of Doppler frequencies f_i ($i = 1, 2$) corresponding to the two fringe systems are described as

$$f_i(u, y) = \frac{u}{d_i(y)}, \tag{1}$$

where u is the velocity of a tracer particle perpendicular to the bisector plane of the beams and $d_i(y)$ are the fringe spacings depending on the position y in the measurement volume. Taking the quotient of the Doppler frequencies yields

$$\frac{f_1(u, y)}{f_2(u, y)} = \frac{d_2(y)}{d_1(y)} = q(y) \tag{2}$$
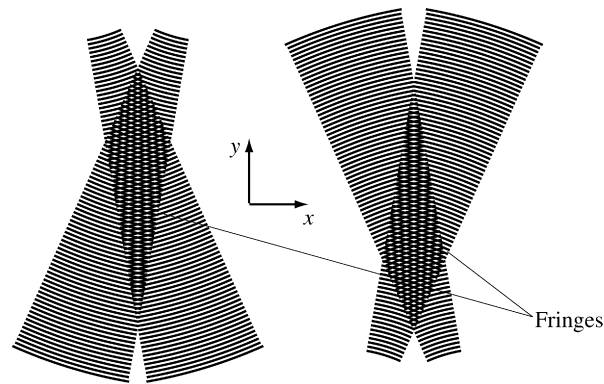
Fig. 2. Fringe systems for realizing a velocity profile sensor. The combination of diverging and converging fringes achieves a high spatial resolution inside the measurement volume in the direction of optical axis (*y*-direction).

as the velocity appearing in the fraction is canceled out. The quotient is only the function of the position inside the measurement volume. So the position can be determined by taking the inverse of the quotient function

$$y = q^{-1}\left(\frac{f_1}{f_2}\right),$$

(3)

as long as the function is known by calibration. Then the velocity can be calculated using Eq. (1). Hence, the sensor provides the position as well as the velocity of individual tracer particles. Since the fringe space curves are unique functions of the coordinate along the optical axis, the position can be precisely known from the calibration without depending on the velocity of the tracer particle. The size of the measurement volume is nearly the same as that of a conventional laser Doppler technique, but high spatially resolved velocity measurement is achieved due to the two fringe systems with different fringe spacing variations without reducing the size of the measurement volume. The positional determination accuracy is proved to be independent of the magnitude of the velocity, and the spatial resolution is ultimately limited by the slope of the calibration curve $q(y)$ and the size of the tracer particle [4]. The relative accuracy of velocity measurement is higher than a conventional LDA because the calibration eliminates the effect of the local fringe spacing variation as discussed in Section 4.

Two different sensor systems were used for the flow measurements. They were realized with different techniques, wavelength-division multiplexing (WDM) and frequency-division multiplexing (FDM), respectively. The difference is the method for discriminating the two fringe systems (refer to [9] for details). Hereafter, they are called as the WDM and FDM sensor based on the techniques, respectively. For the further details of the systems, a reader can refer to [3,4,10] for the WDM sensor and [6,11] for the FDM sensor. The WDM system discriminated the signal from two fringe systems by using two different wavelengths of light, and two different carrier frequencies were used in the FDM system for that purpose. In the following the setup for each sensor system is described in contrast with former setups.

The WDM sensor utilized two single-mode laser diodes with different wavelengths. For the current WDM setup, red and near infrared wavelengths of 658 nm and 784 nm were chosen. The beams from the laser diodes were co-linearly combined by using a dichroic mirror optimized for the two wavelengths. The combined beam was split with a diffraction grating and only the beams of $+1$ and -1 diffraction orders were utilized for creating the measurement volume. The positions of the beam waists were shifted for the two wavelengths in opposite directions to make the fringe patterns convergent and divergent. The scattered light from the measurement volume was collected and the wavelengths were separated with a dichroic mirror before they were guided into photo detectors. In a former WDM system [10], frequency shift was applied with a special frequency stabilization circuit needed to avoid the drift of the shift frequency crucial for the accuracy of velocity measurement. The use of acousto-optic modulators (AOMs) with two wavelengths made it difficult to optimize the adjustment for both wavelengths at the same time. Therefore, the present WDM sensor was not equipped with any frequency shift technique, which is in general aimed at the measurements of reverse flow and small velocity close to zero. However, the measurement of velocity close to the wall was still possible to be accomplished with a method described later on signal processing.

The FDM sensor utilized three AOMs to generate two carrier frequencies. Fiber-optics was used for the robustness and flexibility of the system. The laser source was upgraded to a DPSS (diode-pumped solid-state) laser with an

output optical power of 150 mW, the beam quality of $M^2 < 1.1$ (see [12] for details on M^2) and the rms noise level of less than 0.2% (10–100 MHz) according to the product data sheet. The new laser does not show any spike or noise which hinders precise determination of Doppler frequencies from tracer particles in the flow. The beam quality also increased the incoupling efficiency of the fiber optics and hence the available optical power was much increased in the measurement volume (factor of about five compared to the former system [11]). The beam from the laser was split into four beams and three of them were frequency shifted to 60, 80 and 120 MHz with the AOMs. The frequency shifted beams were guided with single-mode optical fibers into the sensor head. The sensor head was exchanged to a newly designed one with the beams aligned in a plane for improving the signal quality compared to the former one [6]. The beam pairs of 120 MHz and 0 MHz, 80 MHz and 60 MHz were used to realize fringe systems with carrier frequencies of 120 MHz and 20 MHz. The beam waist positions were shifted each other in the direction of optical axis to form converging and diverging fringe systems in the measurement volume. A single photo detector was used and the measured signals were mixed down with the carrier frequencies created from the reference frequency of the AOMs. The pedestal part was removed by the down-mixing before the signal evaluation. The electronics in the former system was not optimized and the measurement was interrupted by high level of noise and parasitic frequencies generated inside the circuit. In the present system [6], the circuit was exchanged with a specially designed circuit with some additional filters for surpressing noise in unwanted frequency ranges. As a result, these upgrades increased the signal-to-noise ratio (SNR) much higher than the former FDM systems and the number of outliers was significantly reduced.

For the signal processing a specially made online processing software was used. The profile sensor was applied with its long side of the measurement volume in the direction of highest velocity gradient so that the velocity profile can be resolved with a high spatial resolution. This yields the occurrence of the particle velocities and hence the Doppler frequencies with much wider dynamic range compared to the case of a conventional LDA applied to a flow region with a high velocity gradient. The ratio of maximum to minimum velocity of at least around 10 should occur in a turbulent boundary layer with the application of a velocity profile sensor. The use of a fixed band-pass filter commonly used for the signal processing of an LDA was known to fail and the use of an adaptive band-pass filter depending on the frequency range of each Doppler burst effectively process such signals with a wide range of frequency occurrence [13]. An algorithm based on the one proposed in [13] was extended with some extra validation steps for the robust determination of the particle position and velocity [5]. In addition, a new processing algorithm was integrated for the WDM sensor not equipped with a frequency shifting technique. In principle, a raw signal is processed by separating the pedestal part from the signal part by using an adaptive band-pass filter in frequency domain. From analytical point of view this is always possible as both peaks have sufficient space in between. The peaks become closer with lower Doppler frequency, but they also scale in width and become narrower. This is because a fast particle with short time duration has a broad spectrum and a slow particle causes a narrow spectrum. So the problem is only the scaling. The adaptive filter technique works, provided that the time record for a Doppler burst is sufficiently long to accommodate both slow and fast particle signals. All the signal processing procedures were realized in self-made program with MATLAB®.

2.3. Calibration

The purpose of the calibration is to obtain the unique relationship equation (1) of the local fringe spacings inside the measurement volume. The fringe spacing can be determined by measuring the Doppler frequencies of the fringe systems using a scattering object with a known velocity passing through the measurement volume. We used a thin metal wire (diameter 4 μm) attached on a rotating wheel as a scattering particle. The wire velocity of the scattering part was known from the rotational radius of the scattering point from the wheel center and the rotational rate of the wheel. The wheel rotation was regulated with a feedback control to maintain the constant rotation rate with nominal accuracy of 5.5×10^{-4}. The wheel was attached on a three-axis precision linear stage. One of the stages was a motorized type and it scanned the measurement volume through y-direction. Several tens of Doppler signal pairs were captured at each position and averaged. The wire was aligned so that it passes through the measurement volume with its tangential path direction identical to x-direction. The effect of curvature on the wire trajectory due to the rotational movement of the wheel was negligible and the wire was regarded to pass straight through the volume as the rotational radius was more than two magnitude larger compared to the diameter of the measurement volume. The scanning through
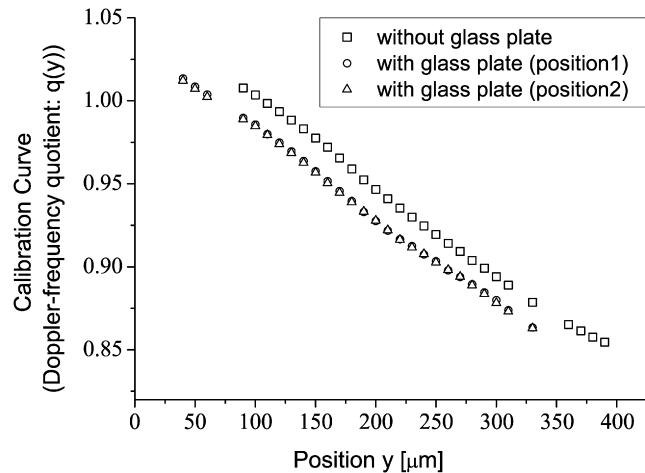
Fig. 3. Effect of glass plate on the calibration curve inserted between the sensor head and the measurement volume. The calibration curve nearly did not change its slope but shifted as long as the sensor is traversed perpendicular to the glass plate.

the measurement volume yielded the local fringe spacings of the two fringe systems in y-direction using polynomial interpolation. The calibration function was calculated by taking the quotient of the fringe spacings.

The effect of the insertion of a glass plate between the sensor and the measurement volume was investigated since a glass plate was used for having optical access in the flow measurements. In general, it shifts the position of the laser beams due to the refraction at the glass surfaces. Care must be taken so that the beams are crossing at a single spatial point to create the measurement volume. As long as the plate is positioned so that the glass surface becomes perpendicular to the optical axis of the sensor, the measurement volume is just shifted in position compared to the configuration without the glass plate being inserted. Fig. 3 shows that the calibration curve remains the same when the glass plate is located at the two different positions 1 and 2, several millimeters apart from each other. It gives an important indication that the calibration curve is not affected by traversing of the sensor. This fact ensures the validity of a single calibration curve for the whole velocity measurement conducted with traversing, as long as the head is traversed perpendicular to the glass plate, i.e., the channel wall. Furthermore, it turned out that the thickness of the glass plate does not cause a serious effect but rather the glass material and possibly surface quality affects the signal quality, hence the effective length of the measurement volume [14]. The calibration of the sensor and the flow measurements were carefully carried out through a glass plate with the same material and thickness as used for the flow measurements.

2.4. Flow measurement

The measurements were conducted with two different sensors at three different Reynolds number conditions. The nominal parameters of the both sensors are listed in Table 1 with the measurement conditions. The coordinates x, y, z were taken so that they correspond to the streamwise, wall-normal, spanwise direction, respectively as shown in Fig. 1. The effective length of the measurement volume was different for the two experimental conditions at $Re_\tau = 420$ and 780 with the same WDM sensor system. This was caused by the quality difference of the glass plates used at these two conditions. Only for the $Re_\tau = 420$ case an optically flat glass plate (surface quality of $\lambda/4$) with anti-reflection coating was employed and otherwise a glass plate with ordinary quality for window made of fused silica was used as described in Section 2.1. The Reynolds number Re_τ was based on the friction velocity $u_\tau = \sqrt{\tau_w/\rho}$ and the channel half-width h with τ_w: wall shear stress, ρ: density. The friction velocity was determined from the streamwise wall-static pressure gradient. The values of the surface roughness at the measurement location made of glass was not measured but were in the same range as the rest of the channel made of aluminum according to the literatures [15–17]. So the wall shear stress at the measurement location was estimated from the other part of fully developed region in the channel without correction. The glass plate with an optical quality at the measurement condition ($Re_\tau = 420$) had a higher surface quality, which was different from the rest of the channel. However, the wall shear stress on the plate was estimated to differ less than 1% from the non-corrected value, which was well within the measurement accuracy

Table 1

Characteristics of the sensors and the measurement conditions (L: working distance, l_x, l_z, l_y: dimension of measurement volume in x, z, y direction, σ_y: spatial resolution, σ_U/U: relative accuracy of velocity measurement, u_τ: friction velocity, $Re_\tau (= u_\tau h/\nu)$: Reynolds number, l_τ: viscous length scale)

Sensor type	L [mm]	$l_x \times l_z \times l_y$ [µm]	σ_y [µm]	σ_U/U [%]	u_τ [m/s]	Re_τ	l_τ [µm]
WDM	80	$100 \times 100 \times 500$	1.5	0.060	0.26	420	60
WDM	80	$100 \times 100 \times 350$	1.5	0.060	0.49	780	32
FDM	310	$100 \times 100 \times 900$	6	0.085	0.71	1100	23

of the wall shear stress as described in the following. The accuracy of the estimation of the wall shear stress and the friction velocity was estimated to be 3∼4% and 2∼3% (with 95% confidence level), respectively. As the length of the measurement volume of the present sensors was not enough to cover the whole measurement region, it was traversed several times to measure the velocity profile from the wall vicinity to the intermediate region.

The three experimental conditions were chosen based on the following concept. The first condition ($Re_\tau = 420$) was chosen focusing on the measurement close to the wall. Hence, the data were collected mainly in the near-wall region. The second condition ($Re_\tau = 780$) was chosen to investigate the use of different glass plates as well as Reynolds number compared to the first case. The third condition ($Re_\tau = 1100$) was chosen to see the effect of the different sensor systems and the Reynolds number compared to the other two conditions. Relatively large amounts of measurement data were taken in the intermediate region for this condition.

The turbulence statistics were calculated using a constant-width slot-technique. Due to the continuous distribution of the data points measured with the velocity profile sensor, the data had to be divided into slots with finite width in order to calculate the statistics. This means that the statistics were calculated for the data points within a certain range of slot with a defined width. The statistics were calculated with the slot overlapped 50%. Hence, each point contributes twice to the statistics. The overlap of 50% was reasonable to reduce the sharp extracting effect at the slot edge on the statistics. A new outlier-reduction scheme based on the local linear fit [14] with a cutoff threshold of four times the standard deviation was applied. The number of points reduced by this scheme was very few out of the total number of data points for each condition. The slot width was empirically chosen for each set of the measurement data so that the statistical convergence and the spatial resolution are balanced. Different widths of slots were applied for mean and higher order moments (rms, skewness, flatness) as listed in Table 2. In the vicinity of the wall, very few samples were collected due to the low density of the tracer particles coming close to the wall. The data sets in several slots close to the wall and the furthest slot from the wall were omitted since there were very few number of data points and the statistical uncertainty increased dramatically in such slots.

A bias-correction scheme was employed using the weighting function based on the inverse of the instantaneous velocity [18] to reduce the velocity biasing effect caused by the steep velocity gradient close to the wall. According to the report on the statistical bias problems in laser anemometry [19], this scheme is not recommended and the scheme based on residence-time weighting should be used. However, residence time was not recorded in the present measurements and the scheme based on the inverse of the instantaneous velocity still did work because the measured velocity component matched the direction of the dominant mean flow.

3. Measurement results

The turbulence statistics of streamwise velocity are shown in Fig. 4 up to fourth order central moment. The statistics shown in Fig. 4 are the mean and rms velocities, third order (skewness factor: $\overline{u'^3}/(\sqrt{\overline{u'^2}})^3$) and fourth order central moments (flatness factor: $\overline{u'^4}/(\sqrt{\overline{u'^2}})^4$) with u' being fluctuating velocity. The mean and rms velocity distributions are normalized with the friction velocity u_τ. The horizontal axis is normalized with the viscous length scale $l_\tau = \nu/u_\tau$. For comparison, available DNS data at $Re_\tau = 640$ by Abe et al. [20] and at $Re_\tau = 400$ and 640 by Iwamoto et al. [21] are shown in the plots. The measurement uncertainties are dominated by the random errors in the flow measurements and the systematic errors of the sensors shown in Table 1 are negligible compared to the statistical ones due to the finite size of samples. The error bars shown in the mean velocity indicate the measurement uncertainty with 95% confidence level. The error bars for the higher order moments indicate the standard deviation calculated by the method described in [22,23].
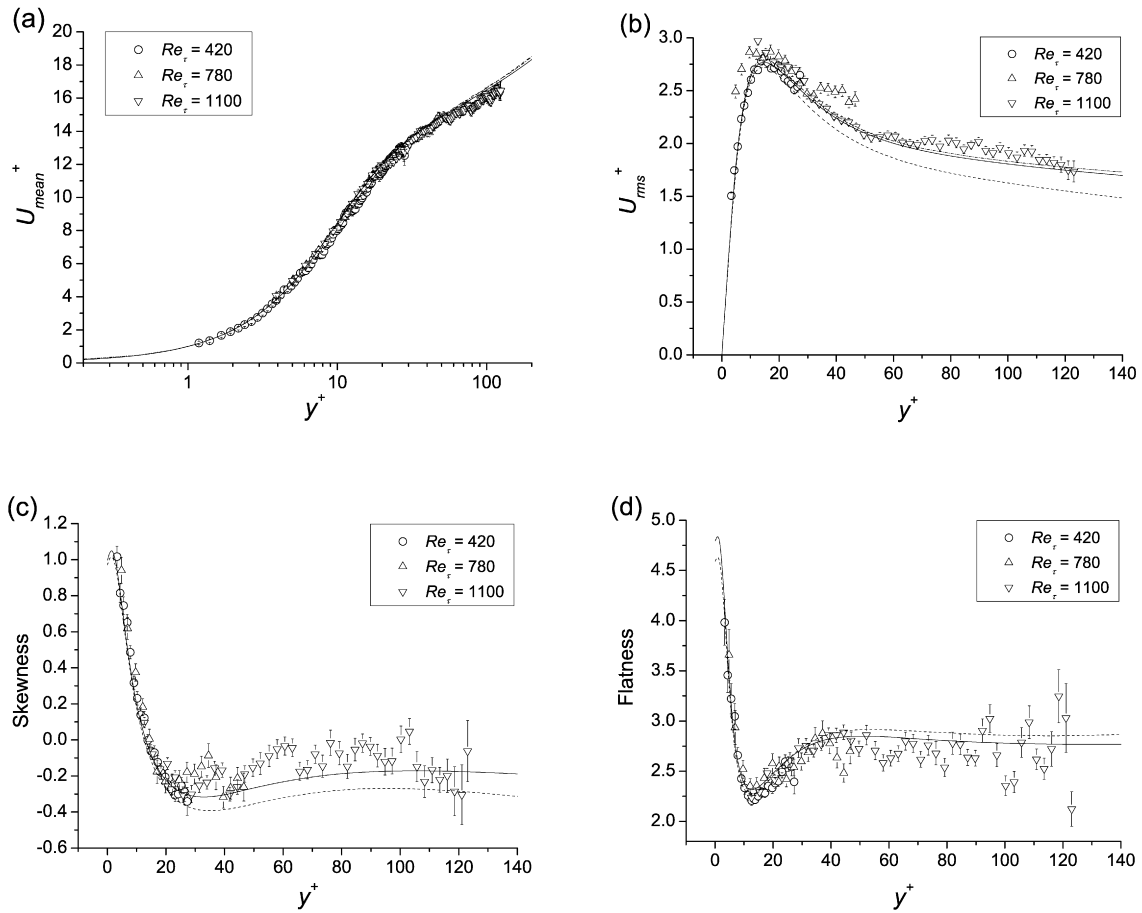
Fig. 4. Turbulence statistics calculated with a slot technique at three different Reynolds numbers compared with available DNS data, $--$: $Re_\tau = 400$ [21], $-\cdot-$: $Re_\tau = 640$ [20], $—$: $Re_\tau = 640$ [21]. (a) mean velocity, (b) rms velocity, (c) skewness factor, (d) flatness factor. The measurement conditions and slot widths used for the statistics are shown in Tables 1 and 2.

Table 2
Slot widths and average number of samples per slot used for calculating the turbulence statistics

Re_τ	mean		rms, skewness, flatness	
	slot width [μm]	sample per slot	slot width [μm]	sample per slot
420	30	400	140	1700
780	80	450	160	850
1100	50	650	120	1450

The mean velocity distributions are shown in Fig. 4(a). They are scaled well with the wall variables and show good agreement with the DNS data. The wall shear stress was estimated also from the near-wall data points with the method [24] using the data points lying in the region $y^+ < 10$. The wall shear stress estimated from the mean velocity shows an excellent agreement with the one estimated from the streamwise pressure gradient within the measurement uncertainties for the lowest Reynolds number condition ($Re_\tau = 420$). In the cases of the two higher Reynolds numbers ($Re_\tau = 780$ and 1100), slight deviations toward higher velocity are observed for the data in the near-wall region. This is supposed to be caused by the remaining effect which could not be corrected by the velocity-bias correction due to the non-equal sampling with particles at different distance from the wall. Another cause was the vibration of the wall as pointed out in Section 4. Relatively small numbers of data points were obtained in the region close to the wall for these two cases. In the highest Reynolds number condition ($Re_\tau = 1100$), the logarithmic velocity profile is

apparently observed in the region apart from the wall, however, it is necessary to collect more number of data points in order to make further statements on this point. It is noteworthy that the velocity data were obtained down to very close to the wall for the lowest Reynolds number case ($Re_\tau = 420$) with the WDM sensor, in which no frequency shifting technique usually employed for measuring small velocity close to the wall was equipped. The closest point obtained for this condition was at $y^+ \approx 1.2$, corresponding to the physical value of 72 μm from the wall and about 0.3 m/s in real scale. This was not due to the limitation of the sensor but rather due to the particle rate and the signal record length used in the measurement.

The rms velocity distributions are shown in Fig. 4(b). They are also scaled well with the wall variables and show good agreements with the DNS data again. The maximum rms values are consistent with generally reported ones. The position of the maximum also coincides well with the position where the turbulence production has its peak in the buffer layer. The present data show some trend of the rms peak depending on the Reynolds number. This might be some possible indication of low Reynolds number effect. The rms statistics show still some scatter in the overlap region, too. This is an indication that more number of data points per slot is required to make further statements on the rms statistics with a high spatial resolution.

The third and fourth order moments (skewness and flatness factors) are shown in Fig. 4(c), (d). They show excellent scalings with the wall variables close to the wall, and the agreement with the DNS data is reasonable. Further comparison of the statistics in the overlap region for different Reynolds number conditions would be possible with more number of data points acquired in the intermediate region for the two lower Reynolds number conditions ($Re_\tau = 420$ and 780). Only the data at the highest Reynolds number condition ($Re_\tau = 1100$) is available in the early part of overlap region and it shows fairly good agreement with the DNS data. The statistics show scatter in the region mainly due to the relatively low number of data points used for calculating the higher order moments. The measured skewness factor shows a systematic deviation compared to the DNS data. The reason for this deviation cannot be explained clearly at this moment, but it should be noticed that the DNS data used for the comparison [21] was at about half the Reynolds number ($Re_\tau = 400$ and 640) compared to that of the present measurement data ($Re_\tau = 1100$). In the DNS data both skewness and flatness factors have a peak close to the wall and their values decrease slightly approaching toward the wall. This behavior was not observed from the present data set due to the lack of data points in the vicinity of the wall and further investigation close to the wall is planned for clarifying this point.

4. Discussion

The velocity profile sensor was demonstrated to be a promising technique for high spatially resolved measurement of turbulence statistics in a turbulent boundary layer. The slot widths used for calculating the statistics from the measurement data were relatively large compared to the full resolution of the sensor. This is because the slot width and the statistical accuracy are in a trade-off relationship with a finite number of data points. It is possible to provide the turbulence statistics with a spatial resolution comparable to that of the velocity profile sensor only when sufficient amount of data is collected in the measurement. To increase the amount of data, one can take mainly two strategies: increasing the particle rate by higher seeding rate or/and spending longer time on the measurement. An important thing is the fact that the profile sensor does not reduce the size of the measurement volume to achieve a high spatial resolution. Therefore, the velocity profile with a high spatial resolution can be obtained without the sensor being traversed and without reducing the data rate. This shortens the time needed for accomplishing a measurement under the same passage rate of tracer particles. The current processing program does not afford to process multiple burst signals occurring at the same time, but in principle, such multiple bursts can be processed as long as they have different Doppler frequencies. If the multiple burst processing is implemented, the data rate would be even increased. The processing possibility and limitation of multiple bursts occurring at the same time is under investigation. An alternative is to use multi-point array detectors with a side scatter regime.

An advantage of velocity profile sensor over conventional techniques is its high accuracy of velocity measurement. Each of the present sensor systems has a relative accuracy of better than 0.1% as shown in Table 1. In general, a conventional LDA has an accuracy of hardly better than 0.5% when whole the measurement volume is used. This is due to the variation of fringe spacing in the direction of optical axis [25]. The accuracy of PIV reported in literature is around the order of 1∼2% for a best optimized condition [26,27]. These values are much lower than that of a velocity profile sensor. The high accuracy of a velocity profile sensor is achieved by the calibration of the fringe spacings and the number of sample points for single Doppler burst signals. The calibration precisely traces the variation of the fringe
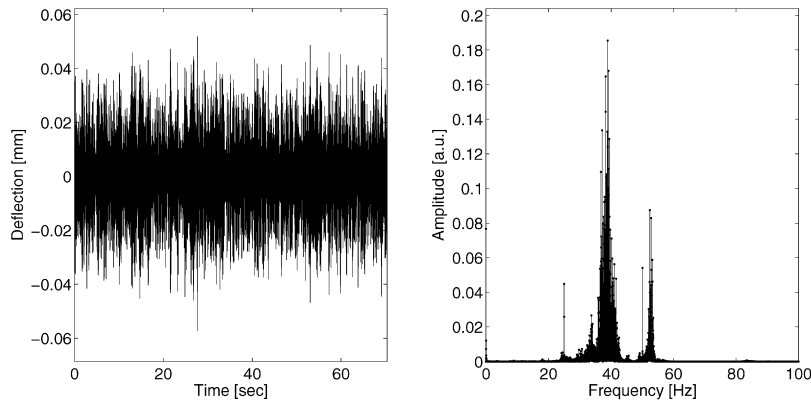
Fig. 5. Typical measurement result of the wall vibration with a laser triangulation sensor at $Re_\tau = 1100$: (a) time signal (left), (b) frequency power spectrum of the time signal (right) (no frequency peaks are observed above 100 Hz).

spacing along the direction of optical axis (*y*-axis). The number of sample points is also an important factor because higher number of samples per burst signal yields better estimation accuracy of Doppler frequency as can be expected from the theory based on Cramer–Rao lower bound [28]. In general, a commercial LDA signal processor takes sample points of maximum at 256 points, which is lower than the points which we normally use for a velocity profile sensor. The number of sample points is in a trade-off relationship with the speed of online signal processing. Use of higher number of sample points degrades the speed of signal processing online, but it achieves the high accuracy of the velocity profile sensor. When a higher speed of data acquisition is required, one can use offline processing as usually done for PIV.

The different realization of the two sensor systems did not yield any discernible difference on the measurement results. Both the sensor systems worked well in the present measurement and can be used for future measurements depending on the requirements on the sensor system. The only differences were the complexity of the systems and the valid data rate during the measurement. The WDM system was simple and relatively easy to be adjusted compared to the FDM system, which utilized complex electronic circuits to operate the AOMs and required careful adjustments of optics. The FDM sensor has a flexibility of the sensor head because of the fiber optics, but more than half of the optical power is lost at the fiber incoupling parts. The valid data rate was lower for the WDM system, while the rate for the FDM system was kept high through the measurement. This was caused by the signal from a particle passing only a single laser beam close to the measurement volume in the case of the WDM sensor. The higher valid data rate for the FDM sensor was achieved by the down-mixing equipped in the FDM system, which effectively reduced such signals from outside the measurement volume before the signal detection.

Providing credible statistical data with the full resolution of a velocity profile sensor is indeed challenging since all the flow conditions must be well controlled to keep the flow state stable during the measurements. Although care was taken for improving the flow boundary condition compared to the former measurement [6], we noticed there was a vibration of the tunnel which appeared beyond certain rotational frequency of the blower. The vertical displacement of the wall at the measurement location was monitored with the same operational conditions as the flow measurement, using a laser triangulation sensor with sample rate of 2.5 kHz and positional resolution of 1 μm. The triangulation sensor was attached to the frame connected to the rigid ground of the laboratory isolated from the frame of the wind tunnel, measuring the position of wall in *y*-direction. Since the sensor was isolated from the wind-tunnel frame, the vibration of the tunnel wall could be evaluated with respect to the velocity profile sensor used in the flow measurement. A typical result of the vibration measurement is shown in Fig. 5 with temporal wall displacement and its frequency spectrum in the direction normal to the flow. It appeared that a periodic oscillation of the wall existed with an approximate frequency of 40 Hz in the wall-normal direction at the high Reynolds number condition ($Re_\tau = 1100$). The effective amplitude of the vibration was ± 13 μm (maximum amplitude: ± 18 μm) and it already exceeded the spatial resolution of the sensor by a factor of 2. Hence the vibration could have influenced on the determination of relative particle position to the wall. On the other hand, its influence on the flow velocity in the channel was supposed to be subtle since the vibration amplitude was smaller in magnitude of at least three compared to the dimension of the channel. When the spatial resolution of a sensor increases, much care has to be taken for the flow condition. The most

probable solution for the channel vibration is to isolate the blower vibration from the channel. If it is not suppressed, one can attach the sensor directly to the wall so that the wall vibration does not change the relative distance from the sensor to the location of the measurement volume inside the tunnel. An alternative is to monitor the wall vibration with the velocity measurement and the wall position can be corrected from the simultaneously taken data. We emphasize that a well controlled flow condition is crucial for such a reliable measurement of turbulence statistics with the high capability of the velocity profile sensor.

5. Conclusion

The application of a velocity profile sensor to the near-wall regions of a fully developed turbulent channel flow was reported. The flow measurements were conducted with the two different sensor systems at three different Reynolds number conditions. The sensor achieved a high spatial resolution of several micrometers range in the wall normal direction by using a combination of converging and diverging fringe systems. Calibration is required to realize high spatial resolution and it is the key for the high accuracy of the velocity measurement of 10^{-3}. The turbulence statistics of the streamwise velocity up to fourth order moment were calculated with a high spatial resolution. The measured mean and rms velocity distributions were scaled well with the wall variables in the near-wall region and showed good agreements with available DNS data. The third and fourth order moments were also measured and showed relatively good agreement with the DNS data. For the higher order moments (rms, third and fourth order moments), even some possible dependence of the statistics on Reynolds number was observed. Both the sensor systems realized with different techniques worked well without giving any discernible difference on the measurement results. It was found that a well controlled flow condition is important to use the full capability of the high spatial resolution achievable with a velocity profile sensor. Acquiring more number of samples with well controlled flow conditions would provide credible data up to higher order moments with the full resolution of the sensors. Such data would give further insights on the detailed structure of turbulence near the wall and possible Reynolds number effects on higher order moments at a high Reynolds number condition. In conclusion, a laser Doppler velocity profile sensor has been demonstrated to be a promising technique for such an investigation of turbulence where a high spatial resolution is required.

References

[1] C.J. Kähler, U. Scholz, J. Ortmanns, Wall-shear-stress and near-wall turbulence measurements up to single pixel resolution by means of long-distance micro-PIV, Exp. Fluids 41 (2006) 327–341.
[2] A. Kempe, S. Schlamp, T. Rösgen, Non-contact boundary layer profiler using low-coherence self-referencing velocimetry, Exp. Fluids 43 (2007) 453–461.
[3] J. Czarske, Laser Doppler velocity profile sensor using a chromatic coding, Meas. Sci. Technol. 12 (2001) 52–57.
[4] J. Czarske, L. Büttner, T. Razik, H. Müller, Boundary layer velocity measurements by a laser Doppler profile sensor with micrometre spatial resolution, Meas. Sci. Technol. 13 (2002) 1979–1989.
[5] C. Bayer, A. Voigt, K. Shirai, L. Büttner, J. Czarske, Interferometrischer Laser-Doppler-Feldsensor zur Messung der Geschwindig-keitsverteilung von komplexen Strömungen, Technisches Messen 74 (2007) 224–234 (in German).
[6] K. Shirai, T. Pfister, L. Büttner, J. Czarske, H. Müller, S. Becker, H. Lienhart, F. Durst, Highly spatially resolved velocity measurements of a turbulent channel flow by a fiber-optic heterodyne laser-Doppler velocity-profile sensor, Exp. Fluids 40 (2006) 473–481.
[7] E.-S. Zanoun, F. Durst, H. Nagib, Evaluating the law of the wall in two-dimensional fully developed turbulent channel flows, Phys. Fluids 15 (2003) 3079–3089.
[8] R.B. Dean, Reynolds number dependence of skin friction and other bulk flow variables in two-dimensional rectangular duct flow, ASME J. Fluids Eng. 100 (1978) 215–223.
[9] J. Czarske, Laser Doppler velocimetry using powerful solid-state light sources, Meas. Sci. Technol. 17 (2006) R71–R91.
[10] K. Shirai, L. Büttner, J. Czarske, H. Müller, F. Durst, Heterodyne laser-Doppler line-sensor for highly resolved velocity measurements of shear flows, Flow Meas. Instrum. 16 (2005) 221–228.
[11] T. Pfister, L. Büttner, K. Shirai, J. Czarske, Monochromatic heterodyne fiber-optic profile sensor for spatially resolved velocity measurements with frequency division multiplexing, Appl. Opt. 44 (2005) 2501–2510.

[12] ISO 11146, Lasers and laser-related equipment – Test methods for laser beam parameters – Beam widths, divergence angle and beam propagation factor, 1999.

[13] K. Shirai, T. Pfister, J. Czarske, Signal processing technique for boundary-layer measurements with a laser-Doppler velocity-profile-sensor, in: Proceedings of the GALA-Fachtagung 13: Lasermethoden in der Strömungsmesstechnik, 6–8th September 2005, Cottbus, Germany, 2005, 4.1–4.8.

[14] K. Shirai, C. Bayer, T. Pfister, L. Büttner, J. Czarske, H. Müller, G. Yamanaka, H. Lienhart, S. Becker, F. Durst, Measurement of universal velocity profile in a turbulent channel flow with a fiber-optic profile sensor, in: Proceedings of the 13th Int. Symp. on Applications of Laser Techniques to Fluid Mechanics, Lisbon, Portugal, 26–29th June 2006, 1.3.1–1.3.12.

[15] I.E. Idel'chik, in: M.O.Steinberg (Ed.), Handbook of Hydraulic Resistance, third ed., Begell House, New York, 1994.

[16] W. Müller, Druckverlust in Rohrleitungen, Energietechnik 7 (1953) 324–326 (in German).

[17] T. Pfister, L. Büttner, J. Czarske, Laser Doppler profile sensor with sub-micrometre position resolution for velocity and absolute radius measurements of rotating objects, Meas. Sci. Technol. 16 (2005) 627–641.

[18] D.K. McLaughlin, W.G. Tiederman, Biasing correction for individual realization of laser anemometer measurements in turbulent flows, Phys. Fluids 16 (1973) 2082–2088.

[19] R.V. Edwards (Ed.), Report on the special panel on statistical particle bias problems in laser anemometry, Trans. ASME J. Fluids Eng., vol. 109, 1987, pp. 89–93.

[20] H. Abe, H. Kawamura, Y. Matsuo, Direct numerical simulation of a fully developed turbulent channel flow with respect to Reynolds number dependence, Trans. ASME J. Fluids Eng. 123 (2001) 382–393.

[21] K. Iwamoto, Y. Suzuki, N. Kasagi, Reynolds number effect on wall turbulence: toward effective feedback control, Int. J. Heat Fluid Flow 23 (2002) 678–689.

[22] A. Stuart, J.K. Ord, Kendall's Advanced Theory of Statistics, vol. 2A: Classical Inference and the Linear Model, Edward Arnold, London, 1994.

[23] L.H. Benedict, R.D. Gould, Towards better uncertainty estimates for turbulence statistics, Exp. Fluids 22 (1996) 129–136.

[24] A. Cenedese, G.P. Romano, R.A. Antonia, A comment on the "linear" law of the wall for fully developed turbulent channel flow, Exp. Fluids 25 (1998) 165–170.

[25] P.C. Miles, Geometry of the fringe field formed in the intersection of two Gaussian beams, Appl. Opt. 35 (1996) 5887–5895.

[26] A.K. Prasad, R.J. Adrian, C.C. Landreth, P.W. Offutt, Effect of resolution on the speed and accuracy of particle image velocimetry interrogation, Exp. Fluids 13 (1992) 105–116.

[27] J. Westerweel, Fundamentals of digital particle image velocimetry, Meas. Sci. Technol. 8 (1997) 1379–1392.

[28] S.M. Kay, Fundamentals of Statistical Signal Processing: Estimation Theory, Prentice-Hall, Upper Saddle River, 1993.